The Cryosphere Discuss., 9, 2135–2166, 2015
www.the-cryosphere-discuss.net/9/2135/2015/
doi:10.5194/tcd-9-2135-2015

The Cryosphere Discussions
Open Access

21st century changes in snow water equivalent over Northern Hemisphere landmasses due to increasing temperature, projected with the CMIP5 models

H. X. Shi and C. H. Wang

Key Laboratory of Arid Climate Change and Disaster Reduction of Gansu Province, College of Atmosphere Science, Lanzhou University, Lanzhou, 730000, China

Received: 4 March 2015 – Accepted: 10 March 2015 – Published: 30 March 2015

Correspondence to: C. H. Wang (wch@lzu.edu.cn)

Published by Copernicus Publications on behalf of the European Geosciences Union.

Abstract

Changes in snow water equivalent (SWE) over Northern Hemisphere (NH) landmasses are investigated for the early (2016–2035), middle (2046–2065) and late (2080–2099) 21st century using twenty global climate models, which are from the Coupled Model Intercomparison Project Phase 5 (CMIP5). The results show that, relative to the 1986–2005 mean, the multi-model ensemble projects a significant decrease in SWE for most regions, particularly over the Tibetan Plateau and western North America, but an increase in eastern Siberia. Seasonal SWE projections show an overall decreasing trend, with the greatest reduction in spring, which is linked to the stronger inverse partial correlation between the SWE and increasing temperature. Moreover, zonal mean annual SWE exhibits significant reductions in three Representative Concentration Pathways (RCP), a stronger linear relationship between SWE and temperature at mid–high latitudes suggests the reduction in SWE there is related to rising temperature. However, the rate of reduction in SWE declines gradually during the 21st century, indicating that the temperature may reach a threshold value that decreases the rate of SWE reduction. A large reduction in zonal maximum SWE (ZMSWE) between 30° and 40° N is evident in all 21st century for the three RCPs, while RCP8.5 alone indicates a further reduction at high latitudes in the late period of the century. This pattern implies that ZMSWE is affected not only by a terrain factor but also by the increasing temperature. In summary, our results show both a decreasing trend in SWE in the 21st century and a decline in the rate of SWE reduction over the 21st century despite rising temperatures.

1 Introduction

As a key component of the cryosphere, snow plays a fundamental role in global climate, due to its high albedo and cooling effect (Vavrus, 2007). However, as global temperatures increase, terrestrial snow cover in the Northern Hemisphere (NH) is changing rapidly. According to the IPCC Third Assessment Report (TAR) (Houghton et al.,

TCD
9, 2135–2166, 2015

2001), the total area of snow-covered land in the NH has decreased by ~ 10 % since the 1960s. Meanwhile, projections of mean annual NH snow cover suggest a further 13 % reduction by the end of the 21st century under the B2 scenario, with individual projections ranging from 9 to 17 % (Meehl et al., 2007). Furthermore, according to the IPCC Fifth Assessment Report (AR5) (Stocker et al., 2013), the total area of NH spring snow cover will decrease by 7 % for Representative Concentration Pathway (RCP) 2.6 and by 25 % for RCP8.5 by the end of the 21st century. From TAR to AR5, although the models' scenarios are different, the area of NH snow cover all represents a declined trend, owing to the fact that snow is highly sensitive to rising temperature. Indeed, several studies have shown that marked decreases in the area and/or depth of snow have already occurred in regions such as western North America (Groisman et al., 2004; Stewart et al., 2005), central Europe (Falarz, 2002; Vojtek et al., 2003; Scherrer et al., 2004) and China (Ji et al., 2012; Wang et al., 2012), thus highlighting the need for better projections of future snow conditions.

The snow depth mainly represents the magnitude of precipitation (snowfall) (Räisänen, 2008), snow cover possibly exhibit a more direct relationship to temperature (Brutel-Vuilmet, 2013). However, snow water equivalent (SWE) primarily reflects the common impact of temperature and precipitation on snow (Räisänen, 2008). According to AR5 (Stocker et al., 2013), the global temperature and precipitation will persistently increase in the 21st century, in order to study the influence of temperature and precipitation on snow, SWE is arguably the most effective tool for assessing the hydrologic impact of snow cover variability (Bulygina et al., 2009), owing to the large number of studies to date. For example, SWE measurements from northwest North America were described by Clark et al. (2001) and have since been used by McCabe and Dettinger (2002) to improve forecasting of seasonal streamflow. Following comparison with observational data, global climate models consistently project declining SWE in many areas by the end of 21st century, while some models shown an increase in snowpack along the Arctic Rim by 2100 (Hayhoe et al., 2004; Brown and Mote, 2009). For example, a 20 km-mesh atmospheric general circulation model projects decreased SWE

TCD
9, 2135–2166, 2015

over much of the NH, and increased SWE over colder regions (Siberia and northernmost North America) due to increasing snowfall during the coldest seasons, although the percentage change of SWE depend on geographical features (Hosaka et al., 2005). Similarly, a regional climate simulation for North America reported increased March SWE in parts of Alaska and Arctic Canada, but decreasing values farther south (Christensen et al., 2007).

According to the Coupled Model Intercomparison Project Phase 3 (CMIP3) projections, changes in seasonal SWE by the end of the 21st century will be spatially variable, with much depending on present local climate conditions (Räisänen, 2008). For example, in very cold regions, climate warming will lead to greater winter snowfall, and thus a thicker snowpack, whereas in warm regions, higher temperatures will result in reduced snowfall. Similarly, CMIP5 experiments project declining SWE over North America south of 70° N (concentrated over the Rocky Mountains, to southern Alaska, and the eastern Canadian provinces), with maximum changes during the peak snow season (January–April), and increasing SWE north of 70° N due to enhanced precipitation (Maloney et al., 2012). Except the influence of climate factor on SWE, Topography also influences variability in SWE. In the mountainous regions of Europe and western North America, projected reductions in SWE are greatest at low elevations (Maloney et al., 2012), but decreases less with increasing altitude, owing to colder winter conditions, while in some areas, simulated SWE actually increase with altitude (Scherrer et al., 2004; Mote et al., 2005; Mote, 2006). Namely, the changes in SWE vary with the altitude.

According to AR5 (Stocker et al., 2013), anthropogenic warming will continue beyond 2100 for all RCPs, with the consequences of accelerating the water cycle and changing the ratio of snowfall to rainfall. Moreover, increased winter precipitation likely will be insufficient to offset the greater contribution of liquid precipitation and enhanced snowmelt driven by higher average temperatures (Räisänen, 2011). From TAR to AR5, projected linear trends in SWE under different scenarios are highly variable since SWE is dependent both on the concentration of total emissions and the duration of emis-

TCD
9, 2135–2166, 2015

sions. Furthermore, several studies conclude that SWE variability can be attributed to either increasing precipitation (Hosaka et al., 2005; Maloney et al., 2012) or temperature (Lemke et al., 2007; Räisänen, 2011), while Räisänen (2008) suggested that the cryospheric response depends on the balance between increasing temperature and precipitation. Consequently, our study was motivated by the need to address the following questions: (1) Throughout the NH scale, how will SWE respond to the different RCPs projected for the 21st century? (2) How about the link between SWE and climate change?

To further analyze anticipated changes in SWE, we employed output from the CMIP5 models in conjunction with GlobSnow product. Here, we focus primarily on temporal and spatial changes in SWE and on variations in the relationship between SWE and climate for each RCP in the 21st century. The specific datasets used in this study are described in Sect. 2, and the comparison between simulated and observed dataset are given in Sect. 3. Temporal and spatial characteristics of SWE are projected and analyzed in Sect. 4, and the relationship between SWE and climate change are discussed in Sect. 5. The main results are summarized in Sect. 6.

2 Datasets

To objectively quantify the changes of SWE in the 21st century, we examined 20 models participating in CMIP5 (Table 1), those all provide monthly SWE variable in the historical experiment and three scenarios experiments (RCP2.6, RCP4.5 and RCP8.5), and we only use the first ensemble member produced by each model (e.g., r1i1p1). While these models vary in their forcing parameters, each model includes the increases in major anthropogenic aerosols observed during the 1850–2005 and anticipated for the future scenarios. Further details are given at http://www-pcmdi.llnl.gov.

The simulations of the models cover the periods 2006–2099 and 2006–2300. Here, we describe changes in SWE during the former period, which is divided into three segments: early (2016–2035: EP), middle (2045–2065: MP) and late (2080–2099: LP)

TCD
9, 2135–2166, 2015

21st century. The analyses were conducted using a 1° × 1° latitude–longitude grid, and re-gridding of original model grids to the analysis grids was conducted via bilinear interpolation.

To verify the performance of the CMIP5 models for simulating SWE, we compared the CMIP5 output with the monthly SWE data from European Space Agency (ESA) GlobSnow dataset (Takala et al., 2011). GlobSnow combines SWE retrieved from passive microwave observation and weather station observation, because of the improved accuracy achieved by assimilating independent sources of information, this is a more realistic SWE product currently available (Hancock et al., 2013). The series cover the period of 1979–2010, and the SWE data have a resolution ratio of 25 km × 25 km, and is also interpolated onto a common 1° × 1° grid. Hereafter, we refer to the GlobSnow dataset as the observed SWE.

3 Validation of CMIP5 simulations for SWE

To evaluate the simulation performance of the models used in this study, we calculated correlations and standard deviation ratios for the observed and simulated winter mean SWE (Fig. 1). We found that each simulated SWE exhibits a close spatial correlation ($P < 0.05$) with the observations, and the majority of standard deviation ratios are close to one. By comparison, most existing models have less-robust correlations and lower standard deviation ratios with the observed data in the time series from 1980 to 2005. However, the multi-model ensembles evidently improve the performance, which have better correlation and standard deviation ratios than the most individual model. In addition, both the observed and the simulated averaged winter mean SWE over the Northern Hemisphere land is also shown in Fig. 2. The observed average winter mean SWE over the Northern Hemisphere is 71.6 kg m^{-2}, while the stimulation ranges from 61.0 to 111.3 kg m^{-2}. Significantly, most models overestimate, and only five models (CanESM2, CSIRO-Mk3-6-0, HadGEM2-ES, MPI-ESM-LR, MPI-ESM-MR) underestimate SWE, compared with the observation, and the multi-model mean is 80.8 kg m^{-2}

TCD
9, 2135–2166, 2015

which is closer to the observation than the most individual model. This illustrates that the multi-model ensemble is more effective for simulating changes in SWE than individual model. From here on, all simulation values denote the multi-model means, and we take the period of 1986–2005 in historical experiment (1850–2005) as the reference period.

4 Changes in SWE in the 21st century

In order to project future patterns of SWE change, we analyze simulations for the three RCPs (RCP2.6, RCP4.5, RCP8.5) on temporal and spatial scales.

4.1 Spatial changes in SWE for the three RCPs

General patterns of projected SWE for the three periods of the 21st century are shown in Fig. 3. Relative to the reference period 1986–2005 (RP), mean annual SWE declines over much of the NH for all the RCPs, with the greatest changes occurring over the Tibetan Plateau (TP). Only in eastern Russia and Siberia does a weak increase in SWE occur. Over North America, above 60° N, we observed a pronounced reduction in SWE during the LP for RCP8.5, with relative-error ratios (RE) ranging from −40 to −10 %, and from −20 to −10 % for both RCP2.6 and RCP4.5. In eastern Siberia, the RE increases to 10 ∼ 20 % for RCP8.5, while for both RCP2.6 and RCP4.5 the RE is less than 10 %. This pattern suggests that, as emissions rise, the intensity of decreased or increased SWE both increases. Meanwhile, we note that the decline in SWE is greater during the LP than during the EP and MP for the same emission scenario. Simulations of mean annual SWE show a similar pattern to those of winter and spring (not shown). For example, in springtime, RE of SWE is between −20 and −10 % over northern North America and ranges from −40 to −20 % over most of Europe. The extent of increased springtime SWE is basically the same as that in winter and the

TCD
9, 2135–2166, 2015

annual mean. Nonetheless, the magnitude of decline of SWE in spring exceeds that in other seasons, resulting that the decrease of SWE in spring is the most significant.

As global temperatures rise, the projected reduction in SWE is most pronounced along the southern limits of seasonal snow cover. Particularly over the TP, where is the unique cold, high-altitude region in the mid-latitude NH (Fig. 3), atmospheric warming serves to accelerate snowmelt and reduce total snowfall amounts (Räisänen, 2008).

To investigate the zonal changes in SWE, Fig. 4 illustrates the zonal changes in mean-annual and maximum SWE and temperature derived from multi-model simulations for the three periods of the 21st century. Relative to RP, the projected temperature increase by the end of the 21st century will not exceed 2 °C for the lower emissions pathway (RCP2.6) (Stocker et al., 2013). However, as indicated by Fig. 4c, f, and i, temperatures will increase more rapidly at high latitude than at lower latitude. Viewed in greater detail, the model results are similar for all three RCPs during the EP, but diverge during the MP and LP. The maximum simulated increase in temperature occurs at high latitude during the LP for RCP8.5.

For all three RCPs, the simulations of mean annual SWE exhibit a clear decline throughout the 21st century (Fig. 4b, e, and h), with the greatest reductions occurring at high latitudes (~ 70–80° N). Relative to RP, the decline in low-latitude SWE during the EP is minor (~ $-10\,\mathrm{kg\,m^{-2}}$) for all three RCPs, and the magnitude of the decline rises with increasing latitude. In contrast, the magnitude of the decline in SWE reaches $-30\,\mathrm{kg\,m^{-2}}$ between 70 and 80° N in each of the three RCPs in EP. While the zonal change in mean annual SWE is highly dependent on RCPs during the MP and LP, particularly at higher latitudes. South of 60° N, the relative changes in SWE during the MP are similar for all three RCPs. However, between 70° and 80° N, the decrease in SWE is $-36\,\mathrm{kg\,m^{-2}}$ for RCP2.6, $-44\,\mathrm{kg\,m^{-2}}$ for RCP4.5, and $-55\,\mathrm{kg\,m^{-2}}$ for RCP8.5. Moreover, the reduction in SWE is more pronounced in the LP than during the EP and MP, particularly for RCP8.5. We note that the maximum increase in temperature and decrease in SWE both occur at high latitudes, suggesting a potential relationship between decreasing SWE and increasing temperature for different RCPs.

TCD
9, 2135–2166, 2015

Figure 4a, d, and g illustrates an intriguing pattern of zonal maximum SWE (ZMSWE) variability. Relative to RP, the ZMSWE exhibits a general decline for all RCPs over the course of the 21st century. However, the ZMSWE shows a similar pattern for the three RCPs during the EP and MP, while the amounts of decline become highly variable during the LP for the three RCPs. This pattern suggests that the change in ZMSWE depends not only on RCP but also on the different periods (e.g., EP, MP, LP). In contrast, a large reduction in ZMSWE occurs between 30 and 40° N for all three RCPs during the EP, MP and LP, and is potentially linked to the strong reduction in SWE over the TP (Fig. 3). As the only cold, high-altitude region in the mid-latitude NH, the unique topographic and cryospheric effects of the TP may have affected the performance of model simulations in this region. Nonetheless, we note the modeled output generally captured the main features of the observations (Fig. 1).

We also note that a second, larger decline in ZMSWE occurs at 60–70° N during LP for RCP8.5, this change always accompanies with the amplified warming at the high latitudes, and the magnitude of this decline in SWE is greater than that at 30–40° N. But this result disagrees with the findings of Brutel-Vuilmet et al. (2008), who suggested that the relative reduction in ZMSWE would be greatest at lower altitudes (20–30° N). According to that study, the low-latitude decline in ZMSWE is driven by strong snowfall reduction, and the changes are weak farther north despite the stronger warming (Brutel-Vuilmet et al., 2008). Other studies also argue that the most significant decrease in ZMSWE occurs at low elevation in mountainous regions (e.g., Maloney et al., 2012); however, the present results In this study show that the significant change in ZMSWE may also occur at higher elevations (e.g., the TP).

As shown in Fig. 4g, the magnitude of the decrease in ZMSWE during the LP for RCP8.5 is greater than for the two lower-emissions pathways (RCP2.6 and RCP4.5), particularly at higher latitude. This pattern also indicates a role for temperature in driving changes in ZMSWE, with the exception of the influence of elevation.

According to AR5 (Stocker et al., 2013), anthropogenic warming will be most pronounced at high latitude, and the temperature increase further leads to changes in

TCD
9, 2135–2166, 2015

water exchange and the water cycle. Additionally, such enhanced warming will influence the rainfall-to-snowfall ratio of winter precipitation, potentially driving changes in snow cover and/or SWE. Table 2 shows projected changes in the zonal relationship between mean annual SWE and temperature. Relative to RP, the rate of decline in mid-latitude SWE will increase with rising temperature for the mid–low emissions pathways. In contrast, the sensitivity of SWE to temperature gradually decreases from the EP to the LP for RCP8.5, suggesting the rate of reduction in SWE might decline as temperature increases beyond a certain level.

In AR4 (Meehl et al., 2007), temperatures in the 40–60° N latitude band were closely correlated with the area of springtime snow cover ($r = -0.68$). This correlation increased to −0.76 in AR5 (Stocker et al., 2013). The present results support those findings, suggesting that the most significant changes in SWE will occur at mid to high latitudes during winter and spring (not shown). Furthermore, the correlation between SWE and temperature is stronger than that reported by AR5 (Stocker et al., 2013), indicating that SWE at mid to high latitudes will persistently decrease with the rising temperature.

4.2 Seasonal changes in SWE

Figure 5 depicts seasonal changes in monthly SWE averaged over the NH landmasses (excluding Greenland) during the RP, EP, MP and LP. The multi-model ensemble shows that simulations during the RP are consistent with the observed SWE, reproducing the basic features of monthly SWE, maximum values during spring, and minimum values during summer. These same features are evident in simulations of the EP, MP, and LP for the three different RCPs, the main difference being that total SWE amounts are lower than those during the RP. Figure 5b, d, and f shows changes in SWE during the EP, MP and LP for all three RCPs, relative to RP. For all three periods of the 21st century, the greatest decrease in SWE occurs during spring, while the smallest reduction occurs in summer, contrary to the pattern of monthly SWE change. The magnitude of the decrease in SWE is similar for each RCP during the EP (Fig. 5b), that is,

TCD
9, 2135–2166, 2015

in the first 20 years of 21st century, the change in SWE relative to RP is the same in all three RCPs, but differences among the RCPs are evident during the MP and LP (Fig. 5d and f). During the LP, the maximum decline reaches $-26.39\,kg\,m^{-2}$ for RCP8.5, while the values range from -13.85 to $-17.45\,kg\,m^{-2}$ for RCP2.6 and RCP4.5, respectively. RCP has stronger effects on SWE change in LP than in EP and MP, although the model uncertainty caused by integration cumulative errors is enlarged from EP to LP. However, the simulation still basically reproduces the features of SWE. Thus, regardless of RCP or time period, the reduction in SWE during the winter half-year exceeds that in the summer half-year, in keeping with the results shown in Fig. 3.

As the dominant parameters influencing SWE, temperature and precipitation both exhibit considerable changes in seasonality (Fig. 6). Relative to RP, temperatures for all three RCPs are projected to rise during the EP (Fig. 6a), MP (Fig. 6c), and LP (Fig. 6e), with the greatest warming occurring in winter, and the smallest in summer. Similar results in EP (Fig. 6a) show that the temperature increase does not exceed 2 °C, which is consistent with the results in AR5. During later periods, the magnitude of warming varies according to RCP, particularly during the LP, for which the RCP8.5 simulation produces a larger change than the other two emissions pathways (Fig. 6e).

Precipitation also exhibits an increasing trend for the different RCPs, with the smallest increase occurring in spring, coincident with the largest decrease in SWE during spring. Simulated changes in precipitation are similar for the different RCPs during the EP (Fig. 6b), but diverge during the MP (Fig. 6d) and LP (Fig. 6f), indicating that the magnitude of projected precipitation changes is dependent on RCP and the time period. The most significant increase in precipitation occurs during the LP for RCP8.5. While the rise in temperature during the winter half-year is larger than that of the summer half-year, the opposite is true for precipitation, with the greatest increase taking place during the summer half-year. This pattern implies that decreasing SWE is attributable to increasing temperature and the minor increase in precipitation.

To differentiate between the relative contributions of temperature and precipitation to SWE, we calculated partial correlations between the SWE and temperature and

TCD
9, 2135–2166, 2015

precipitation. Table 3 shows that for each time period of the 21st century, SWE has a strong negative partial correlation with temperature and weak correlation with precipitation. The significantly negative partial correlation for RCP8.5 decreases from EP to LP in the winter half-year, implying that the rate of decline should diminish as a consequence of rising temperature. We also note that the partial correlation between SWE and temperature during the spring uniformly passes the 90 % significance test during the EP, MP, and LP for RCP8.5, resulting in a persistent decline in springtime SWE. The largest decline in simulated SWE also occurs in spring, consistent with the results shown in Figs. 3 and 5, the decrease in SWE is related to the increasing temperature. Räisänen (2008) proposed that changes in snow conditions will most likely depend on present-day temperature, in close agreement with our results.

The correlation between SWE and temperature in Table 2 reflects the relation of SWE decreasing to the increasing temperature. The sensitivity of SWE to temperature shows a gradually increase over the 21st century form the south to the north. The correlation is significant in most latitude zones (north of 30° N) in EP, but not in MP or LP, in all three RCPs, and is only significant north of 30° N under RCP8.5 in the EP, MP and LP. In addition, SWE is only weakly related to temperature in MP and LP except for several latitude zones in RCP2.6, suggesting that the temperature increase is not always linked to a decreasing SWE.

4.3 Trend changes in SWE

To further analyze the SWE changes in different RCPs, Fig. 7 shows the annual and seasonal SWE trend distribution during 2006–2099 in the NH. The results show that the projected significant changes in SWE occur at mid to high latitudes, with a decreasing trend over the northern North America and the TP, and an increasing trend over Siberia. This pattern shows that the rate of SWE change is spatially variable. The CMIP5 multi-model ensemble projects a decreasing trend in SWE in most regions over the NH landmasses between 2006 and 2099 (Fig. 7). For RCP2.6, the mean annual SWE is projected to decrease considerably over the TP, where the annual mean trend is less

TCD
9, 2135–2166, 2015

than $-4\,\mathrm{kg\,m^{-2}\,(10\,a)^{-1}}$, which is consistent with the temperature increasing rapidly at high elevations in mid-latitude regions. Coastal Alaska is another region where SWE changes are evident, and the trend here is between −1.5 and $-1\,\mathrm{kg\,m^{-2}\,(10\,a)^{-1}}$. In other regions, trends range from −0.5 to $0.5\,\mathrm{kg\,m^{-2}\,(10\,a)^{-1}}$ for RCP2.6. An increasing trend is projected for Siberia.

For RCP4.5, the areal extent of the significant reduction in SWE increases over both the TP and coastal Alaska, and the notably decreasing trend over the TP reflects the decreasing SWE in response to increasing temperature, with the exception of the influence of terrain. For RCP8.5, the mean annual SWE is projected to decline over North America, particularly in western North America and eastern Canada, where the trend is smaller than $-4\,\mathrm{kg\,m^{-2}\,(10\,a)^{-1}}$. In the Eurasia region north of 45° N, SWE is projected to increase in the east (eastern Siberia) and decrease in the west. Another significant negative trend is located over central Russia, where the negative trend in SWE ranges from −3.5 to $-3\,\mathrm{kg\,m^{-2}\,(10\,a)^{-1}}$. At mid–low latitudes in Eurasia, the most significant reductions in mean annual SWE still occur over the TP. Compared with the lower-emissions pathways (RCP2.6, RCP4.5), the magnitude of decline or increase in SWE is greater for RCP8.5. Specifically, the CMIP3 models show that mean annual SWE will increase over eastern regions and decrease over western regions of Eurasia between 2003 and 2060, and that the intensity of SWE changes is greater under higher-emissions scenarios (e.g., A2) than under lower-emissions scenarios (e.g., B1) (Ma et al., 2011).

At the seasonal scale, projected trends in SWE over the NH landmasses are weaker during the summer half-year than the winter half-year for all three RCPs. During winter, in Eurasia north of 45° N, SWE exhibits an increasing trend in the east and a decreasing trend in the west. In contrast, trends in wintertime SWE are uniformly negative over North America and the TP. From the lower emissions to the higher emissions, both the increasing and decreasing trends become more pronounced. In contrast, the extent and intensity of the incremental SWE in winter is larger than that in spring, but the

TCD
9, 2135–2166, 2015

reduction range and strength is significantly smaller than that in spring; consequently, the absolute scale of reduction in SWE is larger in spring than in winter.

Although ensemble simulations show that SWE decreases throughout much of the NH during the three RCPs investigated, we note that there remains a significant increasing trend in SWE across Siberia in winter and spring. Nonetheless, owing to the greater geographical extent and magnitude of the projected reductions, the average trend for the NH in the 21st century is for progressively declining SWE.

The projected changes in mean annual SWE over NH landmasses in the three RCPs are shown in Fig. 8 and Table 4. Relative to RP, mean annual SWE exhibits a consistent decline for each of the three RCPs, with linear trends of −0.54, −1.09, and $-2.05\,\mathrm{kg\,m^{-2}\,(10\,a)^{-1}}$ for RCP2.6, RCP4.5, and RCP8.5 (Table 4), respectively. After 2040, the negative trend in SWE gradually begins to level out for RCP2.6, and weakens somewhat for RCP4.5. For RCP8.5, however, the SWE continues to decline beyond the end of the 21st century, consistent with anticipated reductions in snow cover (Brutel et al., 2012).

5 Changes in SWE with rising temperature

In both seasonal and zonal contexts, rising temperatures play a fundamental role in projected SWE. To analyze the impact of temperature on SWE in the 21st century, the ratios of SWE decrease to temperature increase are calculated for the three RCPs during the EP, MP, and LP (Fig. 9). The ratios reflect the sensitivity of SWE to temperature. Similar linear relations have been reported for sea ice (Mahlstein and Knutti, 2012) and permafrost (Slater, 2013), indicating that increasing temperature plays a central role in cryospheric change. As shown in Fig. 9, the slopes for EP, MP, and LP (-1.47 to $-2.50\,\mathrm{kg\,m^{-2}\,°C^{-1}}$) are less than that for the RP ($-3.17\,\mathrm{kg\,m^{-2}\,°C^{-1}}$), implying that the rate of decrease in SWE ultimately will decline with persistent temperature rise. Furthermore, we note that the sensitivity of SWE to temperature increases gradually from the EP to LP for a single emissions pathway, and over the same period the sensi-

TCD
9, 2135–2166, 2015

tivity decreases when moving from the lower-emissions to higher-emissions pathways. Thus, the impact of temperature on SWE is dependent on the magnitude and duration of emissions forcing.

Furthermore, a linear relationship between SWE and temperature is found for all three RCPs and all three periods (Table 2). The linear regression slope reflects the response of SWE to the increasing temperature. The sensitivity of SWE to temperature gradually declines over the course of the 21st century for RCP8.5, suggesting a threshold for the relationship between SWE and temperature. That is, if the temperature increases to a certain level, the rate of decline in SWE will slow down.

6 Summary and conclusions

We employed twenty CMIP5 climate models to investigate projected changes in SWE for the 21st century, using three different RCPs. We find that, relative to RP, mean annual SWE for all three RCPs exhibits a negative trend over much of the NH landmasses. The most significant reductions occur over the TP and the majority of North America, while a minor increase occurs over Siberia. Moreover, we suggested that the intensity of changes in SWE is greater for RCP8.5 than for RCP4.5 and RCP2.6, and that these changes are most pronounced at mid to high latitudes. Since both the magnitude and geographic extent of the reduction in SWE are much greater in spring than in winter, the overall pattern in the NH is one of declining SWE, with the most significant losses occurring in spring. The multi-model ensemble suggests that the negative trend for RCP2.6 will begin to diminish after 2040, whereas the declining trend continues beyond the end of the 21st century for RCP8.5.

Changes in SWE are accompanied by increasing temperature and precipitation during the winter half-year, most notably in spring. However, the partial correlations between SWE and both temperature and precipitation indicate that considerable decreases in SWE can be attributed primarily to increasing temperatures. Furthermore, we note that while atmospheric warming occurs preferentially during the winter half-

TCD
9, 2135–2166, 2015

year, coincident with the small projected increase in precipitation, but the increase precipitation cannot compensate for the increased snowmelt due to rising temperatures.

Projections of mean annual SWE exhibit declining trends with increasing latitude. Specifically, a more significant reduction in mean annual SWE for all three RCPs occurs between 70 and 80° N for the three time periods of the 21st century, accompanied by an anticipated warming trend. Moreover, the correlation between mean annual SWE and temperature is significant at high latitudes, and the data suggest that a threshold of the relationship between the SWE and temperature would restrain the persistent decline in SWE with increasing temperature. For ZMSWE, the results also show a larger-scale decrease in ZMSWE centered between 30 and 40° N for all RCPs during the three periods investigated, which reflects the influence of terrain on SWE, and other pronounced reduction occurs at high latitude during the LP, only for RCP8.5, implying that, with the exception of topography, changes in ZMSWE are influenced primarily by temperature.

An intriguing feature of the modeled projections is that, although decreasing SWE invariably accompanies the increasing temperature, ratios of SWE decrease to temperature increase are highly variable among the RCPs and modeled time periods. The results suggest that this pattern reflects diminished sensitivity of SWE to temperature during the EP, MP, and LP relative to the RP. As mean annual temperature increases, the rate of decline in SWE will decrease, a pattern that is dependent not only on the specific RCP but also on the time period (e.g., EP, MP, LP). Although the projection results contain uncertainties due to errors caused by integration truncation and inter-model differences, this does not affect the generality or the value of the main conclusions of this study.

Author contributions. C. H. Wang contributed to the idea and conception of this study, analysis of the result and arrangement the framework of the manuscript.
H. X. Shi carried out the analysis of the data and writing the manuscript with the assistance of C. H. Wang.

TCD
9, 2135–2166, 2015

Acknowledgements. This work was supported by the National Natural Science Foundation of China (2013CBA01808), National Natural Science Foundation of China (41275061). The snow water equivalent data used in this study are from European Space Agency (ESA) GlobSnow product and CMIP5 model outputs.

References

Barnett, T. P., Adam, J. C., and Lettenmaier, D. P.: Potential impacts of a warming climate on water availability in snow-dominated regions, Nature, 438, 303–309, doi:10.1038/nature04141, 2005.

Brutel-Vuilmet, C., Ménégoz, M., and Krinner, G.: An analysis of present and future seasonal Northern Hemisphere land snow cover simulated by CMIP5 coupled climate models, The Cryosphere, 7, 67–80, doi:10.5194/tc-7-67-2013, 2013.

Bulygina, O. N., Razuvaev, V. N., and Korshunova, N. N.: Changes in snow cover over Northern Eurasia in the last few decades, Environ. Res. Lett., 4, 045026, doi:10.1088/1748-9326/4/4/045026, 2009.

Clark, M. P., Serreze, M. C., and McCabe, G. J.: Historical effects of El Nino and La Nina events on the seasonal evolution of the montane snowpack in the Columbia and Colorado River Basins, Water Resour. Res., 37, 741–757, doi:10.1029/2000WR900305, 2010.

Falarz, M.: Long-term variability in reconstructed and observed snow cover over the last 100 winter seasons in Cracow and Zakopane (South Poland), Clim. Res., 19, 247–256, 2002.

Groisman, P. Y., Knight, R. W., Karl, T. R., Easterling, D. R., Sun, B., and Lawrimore, J. H.: Contemporary changes of the hydrological cycle over the contiguous United States: trends derived from in situ observations, J. Hydrometeorol., 5, 64–85, 2004.

Hancock, S., Baxter, R., Evans, J., Huntley, B. Evaluating global snow water equivalent products for testing land surface models, Remote Sens. Environ., 128, 107–117, 2013.

Hayhoe, K., Cayan, D., Field, C. B., Frumhoff, P. C., Maurer, E. P., Miller, N. L., and Verville, J. H.: Emissions pathways, climate change, and impacts on California, P. Natl. Acad. Sci. USA, 101, 12422–12427, 2004.

Hosaka, M., Nohara, D., and Kitoh, A.: Changes in snow coverage and snow water equivalent due to global warming simulated by a 20 km-mesh global atmospheric model, SOLA, 1, 93–96, doi:10.2151, 2005.

TCD
9, 2135–2166, 2015

Houghton, J. T., Ding, Y., Griggs, D. J., Noguer, M., vander Linden, P. J., Dai, X., Maskell, K., and Johnson, C. A.: Summary for policymakers, in: Climate Change 2001: the Scientific Basis, Contribution of Working Group I to the Third Assessment Report of the Intergovernmental Panel on Climate Change, Cambridge University Press, Cambridge, UK and New York, NY, USA, 4 pp., 2001.

Ji, Z. M. and Kang, S. C.: Projection of snow cover changes over China under RCPs scenarios, Clim. Dynam., 41, 589–600, 2012.

Ma, L. J., Luo, Y., and Qin, D. H.: Snow water equivalent over Eurasia in next 50 years projected by CMIP3 models, J. Glaciol. Geocryol., 33, 707–720, 2011.

Mahlstein, I. and Knutti, R.: September Arctic sea ice predicted to disappear near 2 °C global warming above present, J. Geophys. Res., 117, D06104, doi:10.1029/2011JD016709, 2012.

McCabe, G. J. and Dettinger, M. D.: Primary modes and predictability of year-to-year snowpack variations in the western United States from teleconnections with Pacific Ocean climate, J. Hydrometeorol., 3, 13–25, 2002.

Meehl, G. A., Stocker, T. F., Collins, W. D., Friedlingstein, P., Gaye, A. T., Gregory, J. M., Kitoh, A., Knutti, R., Murphy, J. M., Noda, A., Raper, S. C. B., Watterson, I. G., Weaver, A. J., and Zhao, Z. C.: Global climate projections, in: Climate Change 2007: the Physical Science Basis, Contribution of Working Group I to the Fourth Assessment Report of the Intergovernmental Panel on Climate Change, edited by: Solomon, S., Qin, D., Manning, M., Chen, Z., Marquis, M., Averyt, K. B., Tignor, M., and Miller, H. L., Cambridge University Press, Cambridge, UK and New York, NY, USA, 772 pp., 2007.

Mote, P. W.: Climate-driven variability and trends in mountain snowpack in western North America, J. Climate, 19, 6209–6220, 2006.

Mote, P. W., Hamlet, A. F., Clark, M. P., and Lettenmaier, D. P.: Declining mountain snowpack in western North America, B. Am. Meteorol. Soc., 86, 39–49, 2006.

Pulliainen, J., Grandell, J., and Hallikainen, M. T.: HUT snow emission model and its applicability to snow water equivalent retrieval, IEEE T. Geosci. Remote, 37, 1378–1390, 2006.

Räisänen, J.: Warmer climate: less or more snow?, Clim. Dynam., 30, 307–319, 2008.

Räisänen, J. and Eklund, J.: 21st Century changes in snow climate in Northern Europe: a high-resolution view from ENSEMBLES regional climate models, Clim. Dynam., 38, 2575–2591, doi:10.1007/s00382-011-1076-3, 2011.

Rawlins, M. A., Willmott, C. J., Shiklomanov, A., Linder, E., Frolking, S., Lammers, R. B., and Vorosmarty, C. J.: Evaluation of trends in derived snowfall and rainfall across Eura-

TCD
9, 2135–2166, 2015

sia and linkages with discharge to the Arctic Ocean, Geophys. Res. Lett., 33, L07403, doi:10.1029/2005GL025231, 2006.
Scherrer, S. C., Appenzeller, C., and Laternser, M.: Trends in Swiss alpine snow days – the role of local and large scale climate variability, Geophys. Res. Lett., 31, L13215, doi:10.1029/2004GL020255, 2004.
Slater, A. G. and Lawrence, D. M.: Diagnosing present and future permafrost from Climate Models, J. Climate, 26, 5608–5623, 2013.
Stewart, I. T., Cayan, D. R., and Dettinger, M. D.: Changes towards earlier streamflow timing across western North American, J. Climate, 18, 1136–1155, 2005.
Stocker, T. F., Qin, D. H., Plattner, G. K., Tignor, M., Allen, S. K., Boschung, J., Nauels, A., Xia, Y., Bex, V., and Midgle, P. M.: Summary for policymakers, in: Climate Change 2013: the Physical Scientific Basis, Contribution of Working Group I to the Fifth Assessment Report of the Intergovernmental Panel on Climate Change, Cambridge University Press, Cambridge, UK and New York, NY, USA, 4 pp., 2013.
Takala, M., Luojus, K., Pulliainen, J., Derksen, C., Lemmetyinen, J., Kärnä, J. P., Koskinen, J., Bojkov, B.: Estimating Northern Hemisphere snow water equivalent for climatic research through assimilation of space-borne radiometer data and ground-based measurements, Remote Sens. Environ., 115, 3517–3529, 2011.
Vavrus, S.: The role of terrestrial snow cover in the climate system, Clim. Dynam., 29, 73–88, 2007.
Vojtek, M., Faško, P., and Šťastný, P.: Some selected snow climate trends in Slovakia with respect to altitude, Acta Meteorologica Universitatis Comenianae, 32, 17–27, 2003.
Wang, Z. L. and Wang, C. H.: Predicting the snow water equivalent over China in the next 40 years based on climate models from IPCC AR4, J. Glaciol. Geocryol., 34, 1273–1283, 2012.

TCD
9, 2135–2166, 2015

Table 1. Models used in this study.

Number	Model	Institution	Resolution
1	BCC-CSM1-1	Beijing Climate Center, China	2.8° × 2.8°
2	BCC-CSM1-1(m)	Beijing Climate Center, China	1.3° × 1.1°
3	CanESM2	Canadian Center for Climate Modeling and Analysis, Canada	2.8° × 2.8°
4	CCSM4	National Center for Atmospheric Research, USA	1.25° × 0.94°
5	CNRM-CM5	Centre National de Recherches Meteorologiques/ Centre Europeen de Recherche et Formation Avancees en Calcul Scientifique	1.4° × 1.4°
6	CSIRO-Mk3-6-0	CSIRO Atmospheric Research, Australia	1.875° × 1.875°
7	FGOALS-g2	Chinese Academy of Sciences	1.4° × 6°
8	FIO-ESM	The First Institute of Oceanography, SOA, China	2.8° × 2.8°
9	GFDL-ESM2G	Geophysical Fluid Dynamics Laboratory, USA	2.5° × 2.0°
10	GISS-E2-H	ASA Goddard Institute for Space Studies, USA	2.5° × 2.0°
11	GISS-E2-R	NASA Goddard Institute for Space Studies, USA	2.5° × 2.0°
12	HadCEM2-ES	Met Office Hadley Centre, UK	1.875° × 1.25°
13	MIROC5	Atmosphere and Ocean Research Institute, Japan	1.4° × 1.4°
14	MIROC-ESM-CHEM	Japan Agency for Marine–Earth Science and Technology, Atmosphere and Ocean Research Institute, Japan	2.8° × 2.8°
15	MIROC-ESM	Japan Agency for Marine–Earth Science and Technology, Atmosphere and Ocean Research Institute, Japan	2.8° × 2.8°
16	MPI-ESM-LR	Max Planck Institute for Meteorology, Germany	1.9° × 1.9°
17	MPI-ESM-MR	Max Planck Institute for Meteorology, Germany	1.875° × 1.875°
18	MRI-CGCM3	Meteorological Research Institute, Japan	1.1° × 1.1°
19	NorESM1-ME	Norwegian Climate Center, Norway	2.5° × 1.875°
20	NorESM1-M	Norwegian Climate Center, Norway	2.5° × 1.875°

TCD
9, 2135–2166, 2015

Table 2. Zonal slope (S) and correlation (C) between SWE and mean temperature for three RCPs. RP, EP, MP, LP represent the periods 1986–2005, 2016–2035, 2046–2065, and 2080–2099, respectively.

			RCP2.6			RCP4.5			RCP8.5		
Lat (° N)		RP	EP	MP	LP	EP	MP	LP	EP	MP	LP
20–30	S	−0.43*	−0.22	−1.45	−0.36	−0.52*	−0.25	−0.08	−0.23*	−0.23*	−0.08
	C	−0.55*	−0.22	−0.42*	−0.14	−0.69*	−0.34	−0.03	−0.45*	−0.48*	−0.30
30–40	S	−2.15*	−4.38*	−0.74	−1.02	−3.39*	−0.85	−2.86	−3.14*	−1.64*	−0.81*
	C	−0.64*	−0.91*	−0.13	−0.13	−0.77*	−0.29	−0.25	−0.84*	−0.78*	−0.68*
40–50	S	−1.00*	−0.84	−1.60	−2.97*	−1.69*	−1.06*	−3.02*	−1.77*	−0.89*	−0.76*
	C	−0.62*	−0.44*	−0.39	−0.55*	−0.80*	−0.48*	−0.71*	−0.86*	−0.74*	−0.82*
50–60	S	−3.27*	−3.82*	−0.39	−2.68	−3.28*	−3.24*	−2.62*	−3.25*	−2.55*	−1.33*
	C	−0.71*	−0.64*	−0.08	−0.28	−0.75*	−0.65*	−0.57*	−0.80*	−0.78*	−0.67*
60–70	S	−2.87*	−2.57*	−2.84	−3.64	−3.67*	−5.10*	−3.71	−4.10*	−3.70*	−2.84*
	C	−0.66*	−0.47*	−0.32	−0.33	−0.74*	−0.76*	−0.35	−0.71*	−0.83*	−0.73*
70–80	S	−10.2*	−16.9*	−0.30	−2.40	−4.57*	−5.23*	−2.10	−8.31*	−6.16*	−4.62*
	C	−0.88*	−0.72*	−0.02	−0.35	−0.65*	−0.81*	−0.06	−0.84*	−0.91*	−0.88*

* Indicate that the slope and correlation exceed the 95 % significance test.

TCD
9, 2135–2166, 2015

Table 3. Partial correlations between SWE and both temperature (T) and precipitation (P) for three RCPs. RP, EP, MP, LP represent the periods 1986–2005, 2016–2035, 2046–2065, and 2080–2099, respectively.

Month		RCP2.6				RCP4.5			RCP8.5		
		RP	EP	MP	LP	EP	MP	LP	EP	MP	LP
Jan	T	−0.29	−0.59*	−0.25	−0.1	−0.54*	−0.44*	−0.52*	−0.45*	−0.38*	−0.31
	P	−0.13	−0.22	−0.05	−0.13	0.1	0	−0.14	0.05	−0.05	−0.05
Feb	T	−0.42*	−0.2	−0.1	−0.37*	−0.25	−0.76*	−0.38*	−0.51*	−0.39*	−0.28
	P	0.05	−0.17	−0.11	0.04	−0.11	0.18	0.09	0.02	−0.05	−0.11
Mar	T	−0.22*	−0.26	−0.24	−0.54*	−0.42*	−0.17	−0.56*	−0.4*	−0.4*	−0.4*
	P	−0.07	−0.03	−0.09	0.22	−0.05	−0.18	0.05	−0.02	−0.03	0.01
Apr	T	−0.38*	−0.31	−0.14	−0.38*	−0.37*	−0.49*	−0.51*	−0.49*	−0.38*	−0.38*
	P	−0.06	−0.1	0.02	−0.01	−0.09	0.09	0.09	0.11	−0.08	−0.05
May	T	−0.36*	−0.33	−0.31	−0.34	−0.31	−0.46*	−0.5*	−0.48*	−0.42*	−0.41*
	P	−0.07	−0.1	−0.38	−0.06	−0.2	0.07	0.09	0.1	−0.06	−0.01
Jun	T	−0.43*	−0.33	−0.57*	−0.07	−0.26	−0.46*	−0.08	−0.45*	−0.39*	−0.38*
	P	−0.07	−0.09	0.12	−0.06	−0.11	0.11	−0.27	−0.04	0.02	−0.05
Jul	T	−0.48*	−0.48*	0.27	−0.26	−0.56*	−0.54*	−0.51*	−0.04	−0.46*	−0.24
	P	−0.11	0	−0.2	−0.14	−0.08	−0.02	0.05	0.02	−0.09	−0.02
Aug	T	−0.33	−0.48*	−0.36*	−0.21	−0.48*	−0.38*	−0.29	−0.47*	−0.48*	−0.4*
	P	−0.07	−0.25	−0.06	−0.03	0	0	−0.02	−0.18	0	−0.06
Sep	T	−0.35	−0.44*	−0.39*	0.13	−0.3	−0.1	−0.59*	−0.27	−0.24	−0.34
	P	−0.05	−0.13	−0.01	−0.14	−0.17	−0.07	0.14	−0.07	−0.15	−0.04
Oct	T	−0.35	−0.53*	0.18	0.16	−0.47*	−0.21	−0.5*	−0.33	−0.28	−0.25
	P	−0.08	0	−0.09	−0.52	−0.03	0.06	0.07	−0.1	−0.06	−0.06
Nov	T	−0.43*	−0.36*	−0.07	0.01	−0.53*	−0.47*	−0.21	−0.29	−0.21	−0.33
	P	−0.05	−0.11	−0.09	−0.28	0.15	−0.05	−0.2	−0.03	−0.17	0
Dec	T	−0.25	−0.5*	−0.12	0.08	−0.27	−0.58*	−0.35	−0.34	−0.28	−0.28
	P	−0.12	−0.05	−0.01	−0.29	−0.16	−0.05	−0.19	−0.03	−0.05	0.04

* Indicate that the partial correlation exceeds the 95 % significance test.

TCD
9, 2135–2166, 2015

Table 4. Trends of SWE during 2006–2099 derived from the three RCPs. Each trend is significant at 95 % confidence.

Trend	RCPs		
$(\mathrm{kg\,m^{-2}\,(10\,a)^{-1}})$	RCP2.6	RCP4.5	RCP8.5
Autumn	−0.51	−1.17	−1.83
Winter	−0.54	−1.18	−2.18
Spring	−0.61	−1.32	−2.39
Summer	−0.50	−1.09	−1.79
Mean	−0.54	−1.09	−2.05

TCD
9, 2135–2166, 2015

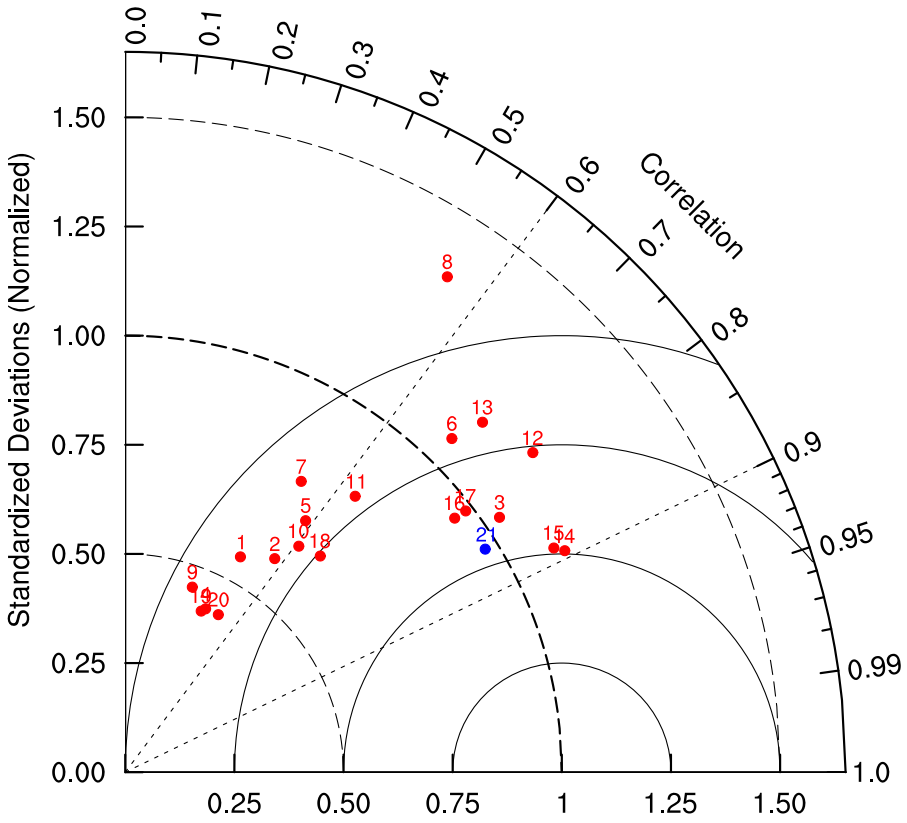

Figure 1. Spatial correlation and standard variance ratios between observed and simulated winter mean SWE during 1980–2005. The serial number 1–20 refers to the model's name in Table 1. The number 21 indicates the multi-model ensemble.

TCD
9, 2135–2166, 2015

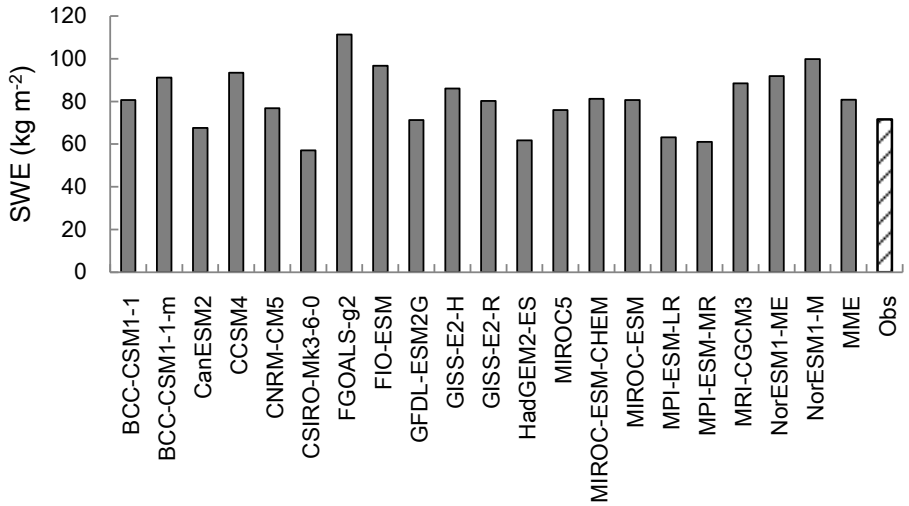

Figure 2. The average of the observed and stimulated winter mean SWE over the Northern Hemisphere land during 1980–2005. (The "MME" comprises the 20 preceding models listed in the figure).

TCD
9, 2135–2166, 2015

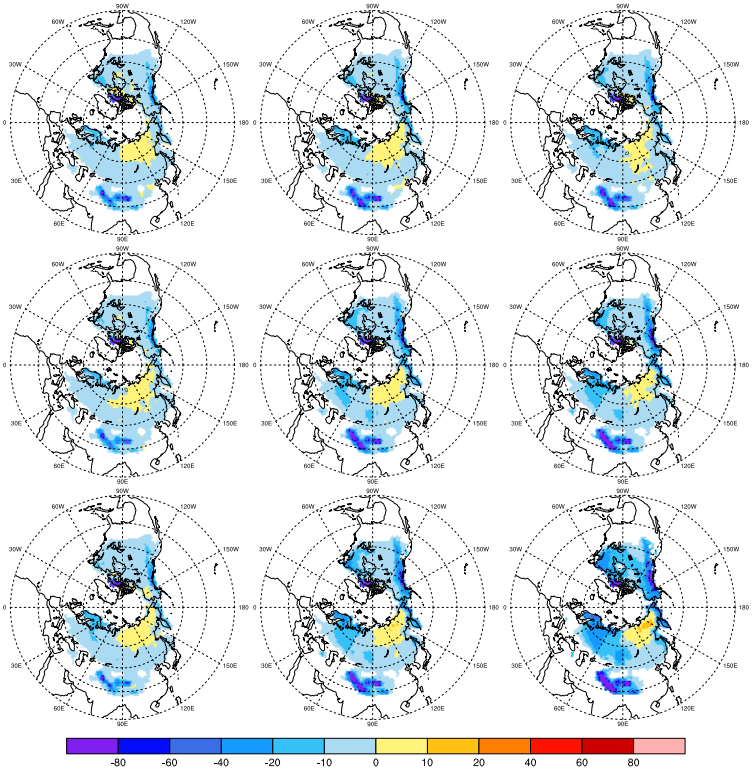

Figure 3. Changes in mean annual SWE ($kg\,m^{-2}$) projected by the CMIP5 ensemble, relative to the 1986–2005 mean. The three rows indicate the three scenarios RCP2.6, RCP4.5 and RCP8.5, respectively, the three columns are the three periods of 2016–2035, 2046–2065 and 2080–2099, respectively.

TCD
9, 2135–2166, 2015

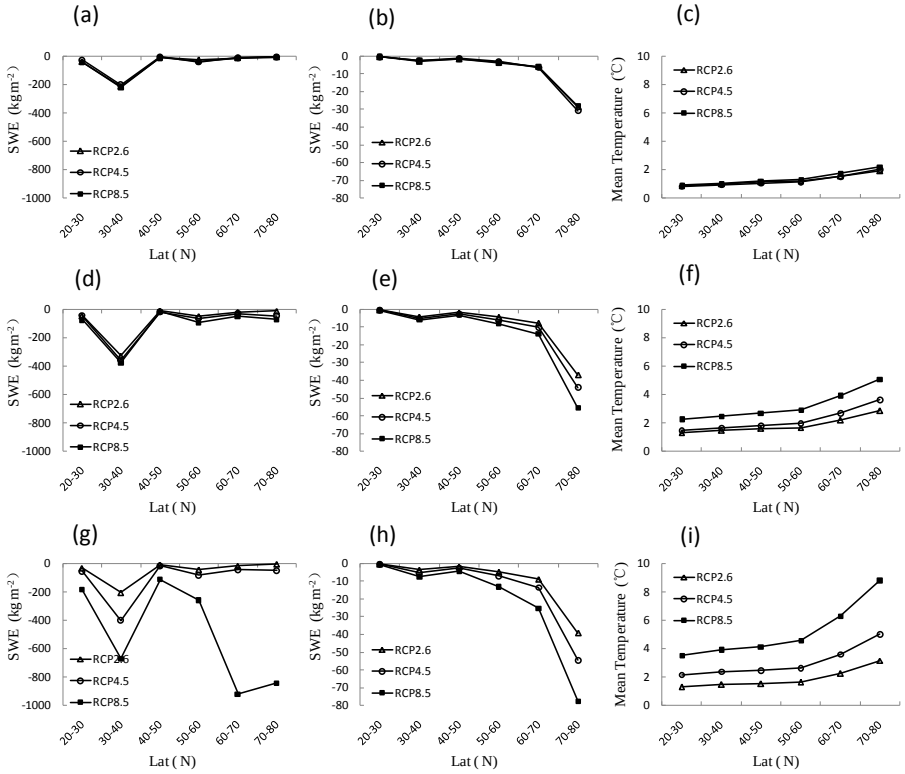

Figure 4. Zonal changes in maximum annual SWE (panels **a**, **d**, **g**), mean annual SWE (panels **b**, **e**, **h**), and mean annual air temperature (panels **c**, **f**, **i**) for 2016–2035 (top), 2046–2065 (middle), and 2080–2099 (bottom), relative to the 1986–2005 mean.

TCD
9, 2135–2166, 2015

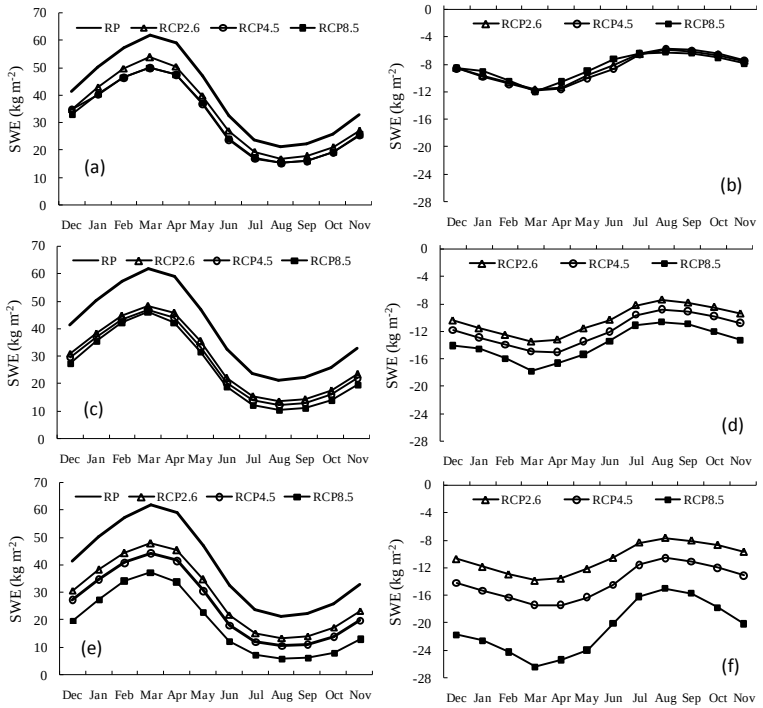

Figure 5. Projected changes in monthly average SWE over NH landmasses: panels **(a)**, **(c)**, and **(e)** show the output of the RP (1986–2005), RCP2.6, RCP4.5, and RCP8.5 simulations; panels **(b)**, **(d)**, and **(f)** depict changes in SWE, relative to RP, for 2016–2035 (top), 2046–2065 (middle), and 2080–2099 (bottom).

TCD
9, 2135–2166, 2015

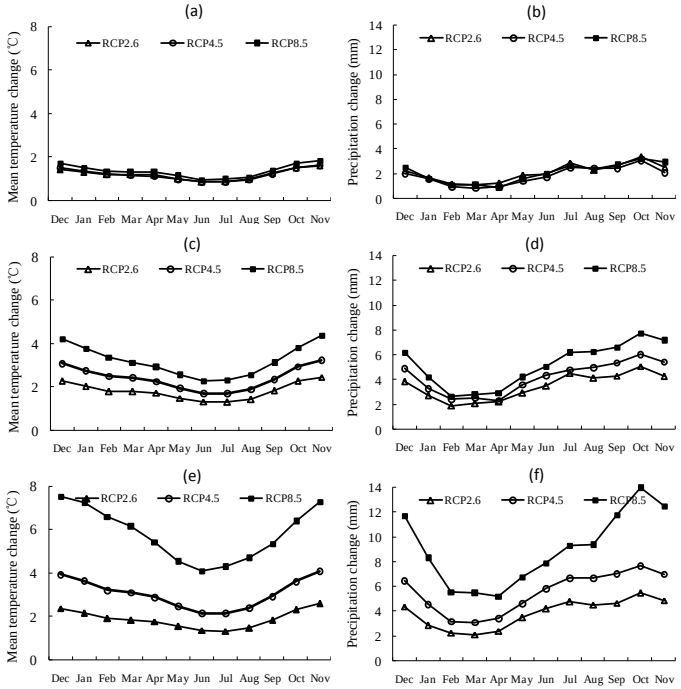

Figure 6. Changes in mean annual air temperature (left) and precipitation (right) for 2016–2035 (**a** and **b**), 2046–2065 (**c** and **d**), and 2080–2099 (**e** and **f**), relative to the 1986–2005 mean, for three RCPs.

TCD
9, 2135–2166, 2015

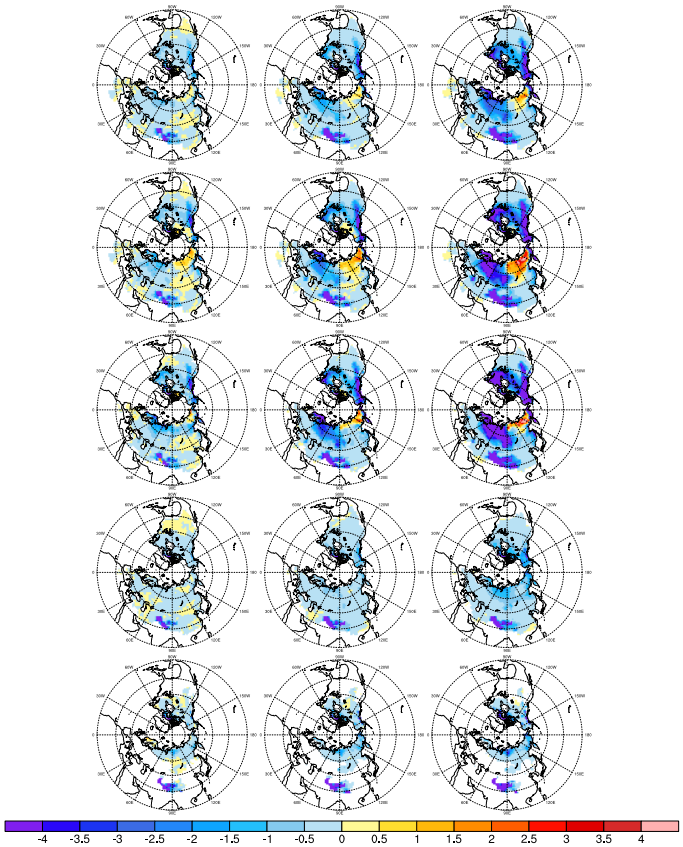

Figure 7. Spatial distributions of projected SWE trends ($kg\,m^{-2}\,(10\,a)^{-1}$) between 2006 and 2099 for the three RCPs. Shaded areas represent regions where trends reach 95 % significance. The five rows indicate the annual mean, winter, spring, summer, and autumn SWE. The three columns are RCP2.6, RCP4.5, and RCP8.5, respectively.

TCD
9, 2135–2166, 2015

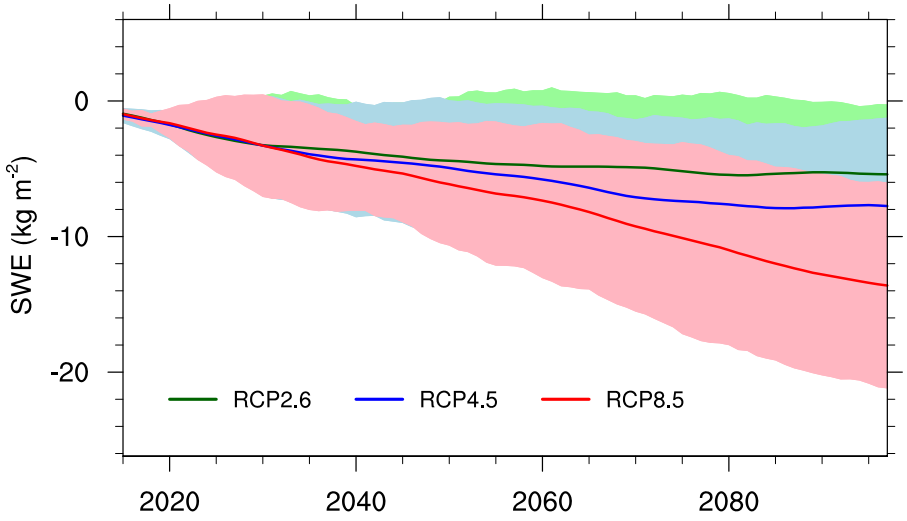

Figure 8. Projected changes in mean annual SWE over NH landmasses during 21st century, relative to RP (1986–2005), for all three RCPs (green: RCP2.6; blue: RCP4.5; red: RCP8.5). Also shown is the multi-model mean for all available models for each scenario. The 10 yr running average is derived for each model before calculation of the multi-model mean. Shaded areas denote the inter-model standard deviation for each ensemble mean.

TCD
9, 2135–2166, 2015

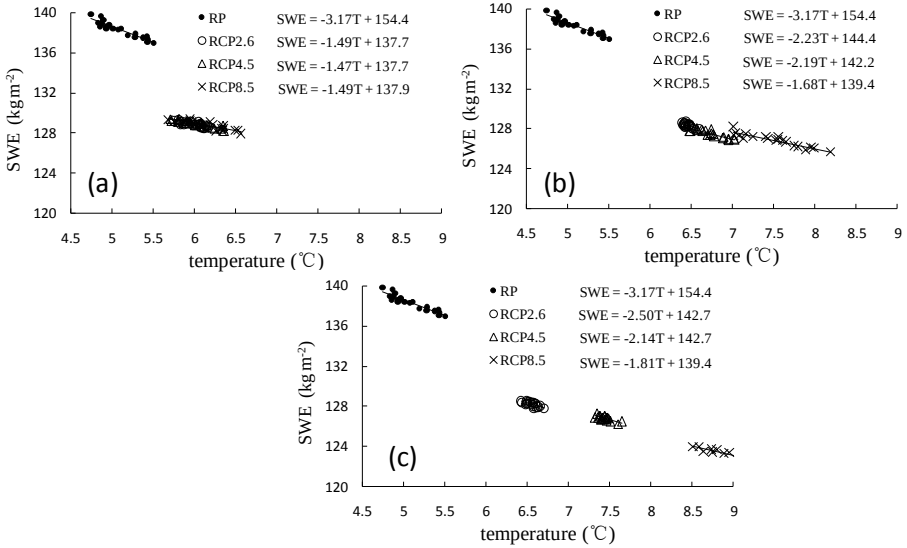

Figure 9. Sensitivity of SWE to mean annual temperature over NH landmasses, derived from three RCPs, for the periods 2016–2035 **(a)**, 2046–2065 **(b)**, and 2080–2099 **(c)**. The term "RP" indicates the reference period of 1986–2005.

TCD
9, 2135–2166, 2015